Spherical Non-LTE Line-Blanketed Stellar-Atmosphere Models of the Early-B Giants ϵ CMa, β CMa, and α Vir

J. P. Aufdenberg

Department of Physics and Astronomy, Arizona State University, Tempe, AZ 85271-1504, USA

P. H. Hauschildt

Department of Physics and Astronomy & Center for Simulational Physics, University of Georgia, Athens, GA 30602-2451, USA

E. Baron

Department of Physics and Astronomy, University of Oklahoma, Norman, OK 73019-0225, USA

Abstract. We model the full multi-wavelength spectra, including the extreme ultraviolet (EUV) continuum, of three early-B giants, ϵ CMa, β CMa, and α Vir, with spherical, non-LTE, fully line-blanketed model atmospheres. Comparisons of these models to the spectrophotometric data, along with the HIPPARCOS parallax measurements, provide fundamental stellar parameters for these stars. We find close agreement between the models and the measured EUV fluxes from ϵ CMa and β CMa as a result of the higher temperatures at the formation depths of the H I and He I Lyman continua compared to other models. The realistic model treatment of early-B giants with spherical geometry and non-LTE metal line blanketing results in the prediction of significantly larger EUV fluxes compared with plane-parallel models.

1. Introduction

Model-atmosphere flux distributions of hot luminous stars are generally in good agreement with the observed fluxes longward of 912Å. Until very recently, however, the lack of spectroscopic data in the extreme ultraviolet (EUV) has left models untested in this wavelength region. The early B-type stars β CMa and ϵ CMa are the only two hot luminous stars that have been observed shortward of the Lyman edge (Cassinelli et al. 1995, 1996). These direct observations provide an opportunity to compare directly the observed EUV flux distributions of hot stars with those predicted by model atmospheres. These stars have exhibited an 'EUV excess' relative to the predictions of hydrostatic plane-parallel, as well as dynamic and extended, line-blanketed, LTE and non-LTE model-atmosphere calculations (Cassinelli et al. 1995, 1996; Najarro et al. 1996; Schaerer & de Koter 1997).

Spectroscopy of the bright B2 II star ϵ CMa (HD 52089, HR 2618; Cassinelli et al. 1995) below the Lyman edge by the Extreme Ultraviolet Explorer (EUVE) satellite is possible due to the extremely low neutral-hydrogen column density toward this star. As a result of its location at a HIPPARCOS distance of 132^{+11}_{-9} pc along an exceptionally rarefied interstellar tunnel extending out from the 'Local Bubble' (Welsh 1991), ϵ CMa is attenuated by a neutral-hydrogen column density of less than 5×10^{17} cm^{-2} (Gry et al. 1995). Consequently, it is an extremely important contributor to local interstellar-hydrogen ionization.

The bright B2 II–III star β CMa (HD 44743, HR 2294) was observed spectroscopically below the Lyman edge by EUVE (Cassinelli et al. 1996). Located at a HIPPARCOS distance of 153^{+17}_{-14} pc, β CMa is attenuated by a neutral-hydrogen column density of less than 2×10^{18} cm^{2} (Gry, York, & Vidal-Madjar 1985). The effective temperature of β CMa has been uncertain due to the inability of previous LTE or non-LTE stellar-atmosphere models to simultaneously match the observed flux from the EUV through the infrared.

The Lyman continuum of the B1.5 IV–V primary in the α Vir system (HD 116658, HR 5056) was not detected in two EUVE pointed observations. The detection of a very faint emission nebula surrounding α Vir by Reynolds (1985), however, puts a *lower* limit on the ionizing flux from α Vir. Adopting the HIPPARCOS distance to α Vir, $d = 80^{+6}_{-5}$ pc, the lower limit on α Vir's Lyman continuum luminosity from Reynolds (1985) is $Q_0 = 1.6 \pm 0.6 \times 10^{46}$ photons s^{-1}.

In this contribution we present PHOENIX non-LTE model atmospheres and synthetic spectra for the early B stars ϵ CMa, β CMa, and α Vir. We discuss the comparisons of these models with the observed spectrophotometry and show that together with recently released HIPPARCOS parallax measurements these comparisons provide fundamental parameters for these stars. We discuss differences between our line-blanketed, plane-parallel and spherical model atmospheres, which appear to explain a large part of the reported discrepancy between the observed EUV flux of early B giants ϵ CMa and β CMa, and the EUV flux predicted by plane-parallel LTE and non-LTE line-blanketed model atmospheres.

2. Description of the Stellar-Atmosphere Models

We have computed models using the generalized stellar-atmosphere computer code PHOENIX (version 8.1), which calculates LTE and non-LTE, line-blanketed, spherical expanding model atmospheres (Hauschildt et al. 1995; Hauschildt et al. 1996; Hauschildt, Baron & Allard 1997; Baron & Hauschildt 1997, and references therein). The PHOENIX code can handle very large non-LTE model atoms as well as line blanketing by millions of atomic (and molecular) lines. This code is designed to be very flexible. It has been used to compute model atmospheres and synthetic spectra for novae; supernovae; white, brown, and M dwarfs; and accretion disks in active galactic nuclei.

We have computed four different classes of models: LTE; non-LTE with H and He but without metal-line blanketing; non-LTE including ions of H, He, C, N, and O; and non-LTE models including ions of H, He, C, N, O, Ca, Mg, and Fe. All models include the effects of statistical (random) velocity fields using a

Gaussian broadening velocity of $\xi = 2$ km s^{-1}. Details of the four classes are as follows:

(*i*) A large number of ionization stages is required to span the wide range of electron temperatures and gas pressures encountered in OB-star atmospheres. Typical LTE models (and non-LTE models which consider background line-blanketing in LTE) use lines from ions of H, He, Li, Be, B, C, N, O, F, Ne, Na, Mg, Al, Si, P, S, Cl, Ar, Ca, Sc, Ti, V, Cr, Mn, Fe, Co, Ni, Cu, Zn, Ga, Kr, Rb, Sr, Y, Zr, Nb, Ba, and La, selected from Kurucz (1994). Approximately 2.1×10^6 background LTE lines are considered in these models. The model is computed on a grid of 11 074 wavelength points. The LTE models are calculated starting from an LTE-grey model and iterated to convergence.

(*ii*) A non-LTE pure H-He model with no metal-line blanketing uses 101 levels, producing 545 transitions from H I and He I–II. The models are computed on a grid of 13,569 wavelength points. The models are started from an LTE-grey model structure and iterated to convergence.

(*iii*) A typical non-LTE H-He-CNO model considers 1 751 levels, producing 11 975 transitions from H I, He I–II, C I–IV, N I–VI, and O I–VI in detailed non-LTE in addition to the background LTE line blanketing discussed above. The models are computed on a grid of 63 486 wavelength points. The non-LTE models are calculated starting from a converged LTE line-blanketed model and iterated to convergence.

(*iv*) More complete non-LTE models employ 3 035 levels, with 37 151 transitions from the ions H I, He I–II, C I–IV, N I–VI, O I–VI, Ca II, Mg II, and Fe II–III in detailed non-LTE in addition to the LTE line blanketing. These models are computed on a wavelength grid of 183 591 wavelength points. The models are calculated starting from a non-LTE H-He-CNO-class model. The models of ϵ CMa, β CMa, and α Vir are of this type.

3. Results

3.1. ϵ CMa

A synthetic spectrum is compared with the observed spectrum of ϵ CMa in Fig. 1. A plane-parallel LTE ATLAS9 model ($T_{\rm eff} = 21000$ K, $\log g = 3.2, \xi = 2$ km s^{-1}) (Kurucz 1992) is shown for comparison. Our model reproduces the strengths of the 912Å and 504Å edges; however, it does not reproduce the observed slope in the EUV spectrum below 504Å. Effects of a stellar wind and non-thermal heating processes may alter the ionization structure of the atmosphere and population of the He I ground state; for more details see Aufdenberg et al. (1997).

The effective temperature of the ϵ CMa model, $T_{\rm eff} = 21\,750$K, is at the limit of the established range in the measured effective temperature, $T_{\rm eff} = 20\,990 \pm 760$K (Code et al. 1976). This effective temperature, derived from the bolometric flux distribution, may be subject to a small but significant systematic errors. The far-UV flux from ϵ CMa (between 2300Å and 2800Å), measured by the Goddard High Resolution Spectrograph (GHRS), is $\sim$30% higher than that measured by OAO-2. Adopting the GHRS flux we calculate an effective temperature of 21500$\pm$780 K, closer to the best-fitting model effective temperature.

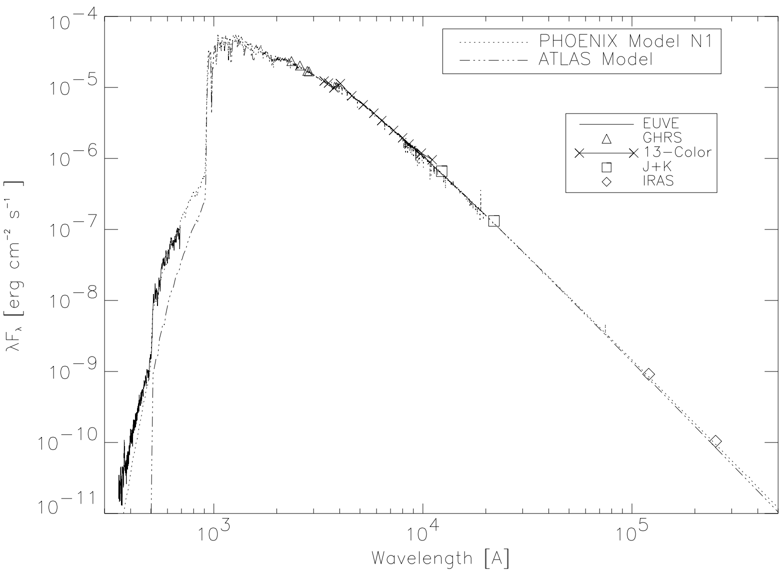

Figure 1. The continuous energy distribution of ϵ CMa from 350Å to 25μm compared with the 21 750 K non-LTE model (N1) and the ATLAS9 21 000 K model. The EUVE data are corrected for interstellar neutral-hydrogen column assuming a neutral-hydrogen column density of $N(\mathrm{H}^0) = 5 \times 10^{17}$ cm^{-2}.

The model surface gravity, $\log g = 3.2$, and angular diameter, $\theta = 0.77$ mas, are within established limits: $\log g = 3.20 \pm 0.15, \theta = 0.80 \pm 0.05$ mas (Cassinelli et al. 1995). In light of the HIPPARCOS distance to ϵ CMa, however, a surface gravity of $\log g = 3.2$ appears to be too low by approximately 0.3 dex. Based on a comparison with the evolutionary tracks (see Fig. 2), ϵ CMa has a mass of nearly $12 M_\odot$, however, the measured radius, with a gravity of $\log g = 3.2 \pm 0.15$, yields a mass of $7.4 \pm 3.0 M_\odot$. atmosphere models computed with $\log g = 3.5$ do not show a significantly different EUV flux distribution. A possible resolution to this mass discrepancy may be found from a reanalysis of the Balmer line fits (Cassinelli et al. 1995) used to establish the surface gravity.

3.2. β CMa

A synthetic spectrum of our β CMa model is compared with the observed spectrum in Fig. 3. The synthetic spectrum is scaled to match the observed optical and near-IR spectrophotometry by adopting an angular diameter of 0.57 mas. A plane-parallel LTE ATLAS9 model ($T_{\rm eff} = 23\,250$ K, $\log g = 3.4, \xi = 2$ km s^{-1}, $\theta = 0.59$ mas) (Kurucz 1992) is shown for comparison and scaled in the same way. The effective temperature of the β CMa model is at the edge of the range in the measured effective temperature $25\,180 \pm 1\,130$ K (Code et al. 1976). This effective temperature, like that of ϵ CMa, may too be subject to small but significant systematic errors due to the adopted absolute calibration in the UV.

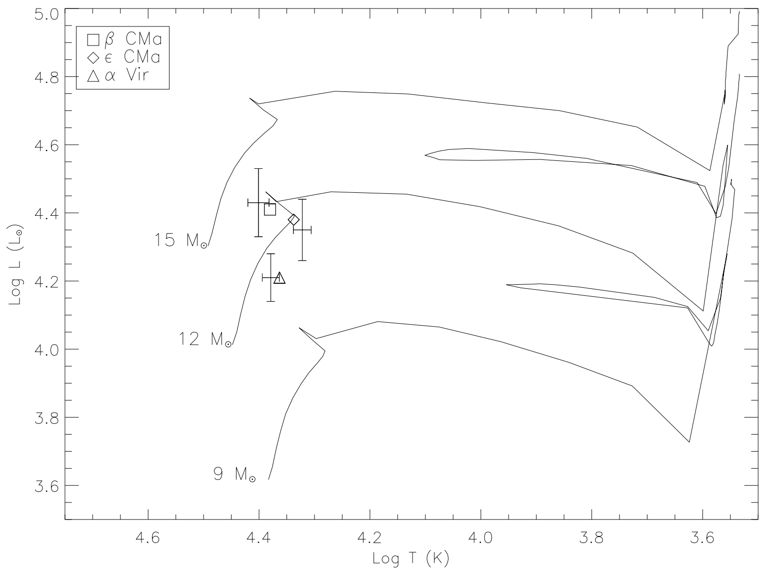

Figure 2. The locations of ϵ CMa, β CMa, and α Vir plotted along with the evolutionary tracks by Schaller et al. (1992) in the theoretical HR diagram. The error bars reflect the 1-σ errors in the measured total flux and the measured angular diameter (Code et al. 1976), and the standard error in the HIPPARCOS parallax. The symbols represent the best-fit values based on the comparison of the synthetic spectra to the spectrophotometry adopting the mean HIPPARCOS distance.

We find a neutral hydrogen column density of $N(\mathrm{H}^0) = 2 \times 10^{18}$ cm^{-2} provides the best match between the observed and synthetic continua. Our model spectrum closely reproduces the H I Lyman continuum observed by EUVE while the comparison ATLAS9 model continuum, in agreement with the observed flux distribution longward of 912Å, is about a factor of 3 smaller than the observed EUV continuum for the adopted neutral column density.

We do not correct the EUVE data for the interstellar He^0 column. It is likely that the stellar He I continuum is not detected by EUVE, but instead the observed signal below the He I 504Å edge is the result of scattered light within the EUVE spectrograph (Cassinelli et al. 1996). Comparing the observed flux below the 504 Å edge to the flux predicted by our model, we find a lower limit on the interstellar neutral helium column toward β CMa of $N(\mathrm{He}^0) \geq 5.8 \times 10^{17}$ cm^{-2}.

Figure 2 shows β CMa plotted on a theoretical HR diagram. Based on a comparison with the evolutionary tracks, β CMa has a mass near $12 M_\odot$. This mass is at odds with that determined from the measured radius and spectroscopic gravity. A gravity of $\log g = 3.4 \pm 0.15$, $\theta = 0.52 \pm 0.03$ mas (Code et al. 1976), and the HIPPARCOS distance, yield a mass of $6.7 \pm 2.8 M_\odot$. Our model fits to the Balmer line profiles (Watson 1972) are consistent with $\log g = 3.4$. Part of this mass discrepancy may be that the angular diameter is systematically too

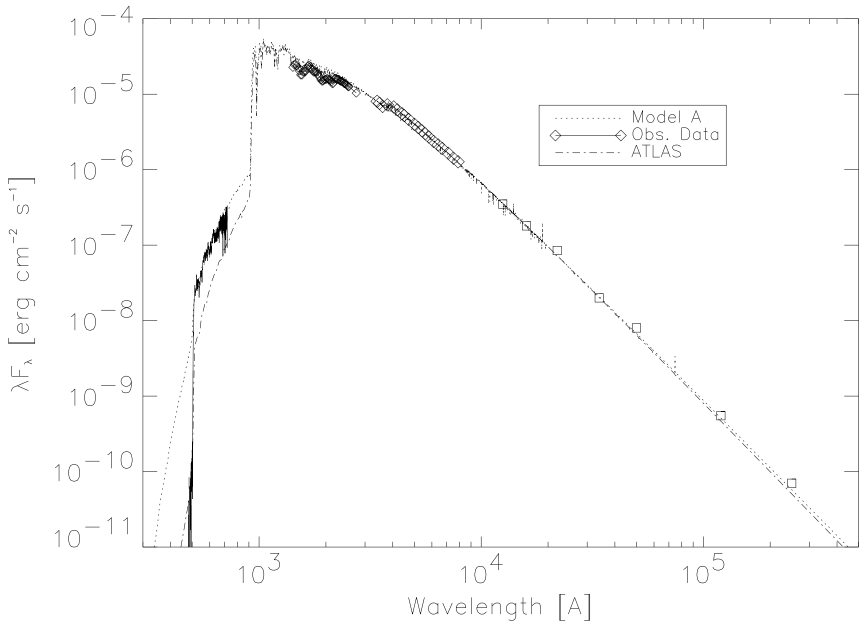

Figure 3. The continuous energy distribution of β CMa from 500Å to 25μm compared with the 24 000 K non-LTE model (model A) and the ATLAS9 23 250 K model. The EUVE data are corrected adopting a neutral-hydrogen column density of 2×10^{18} cm^{-2}. The observed spectrum below 504Å is not a realistic stellar continuum due to absorption by the interstellar He I column, which is not corrected for here.

small. Our model best fits the spectrophotometry with an angular diameter of $\theta = 0.57$ mas.

3.3. α Vir

A synthetic spectrum from our α Vir model is in good agreement with the IUE, corrected OAO-2 (Bohlin & Holm 1984), and optical spectrophotometric data from 1200Å to 8000Å. The comparison of these data sets with our α Vir model is shown in Fig. 4. No correction for interstellar extinction and reddening are made to these data due to the extremely low reddening toward α Vir.

Our best fitting model parameters are $T_{\rm eff} = 23\,070$ K, $\log g = 3.6$, and $\theta = 0.93$ mas. This effective temperature is near the limit of the measured range, $T_{\rm eff} = 23\,930 \pm 840$ K (Code et al. 1976). Smalley & Dworestsky (1995) compute a *smaller* effective temperature, $T_{\rm eff} = 23\,070 \pm 1\,000$ K, but consider a *larger* flux ratio between the primary and secondary components of this binary system than Code et al. (1976), which suggests the uncertainty in α Vir's effective temperature is probably slightly larger than shown in Fig. 2. The dynamical mass ($10.8 \pm 1.3 M_\odot$, Popper (1980)), spectroscopic mass ($9.2 \pm 1.5 M_\odot$), and evolutionary mass (11–$12 M_\odot$) are basically consistent. The slightly larger angular diameter, relative to the measured value ($\theta = 0.87 \pm 0.04$; Code et al.

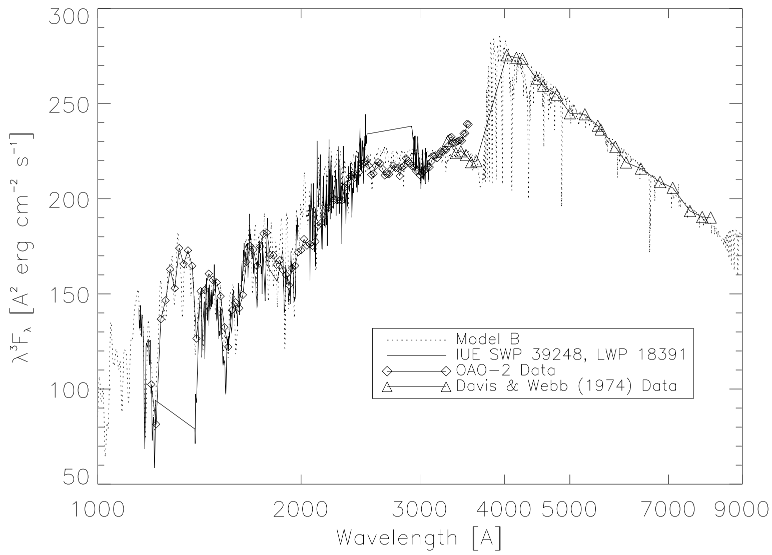

Figure 4. A comparison of the IUE low-dispersion data, corrected OAO-2 data, and optical spectrophotometry of α Vir with the 23 070 K non-LTE model (model B). The IUE data between 1215–1400Å, 1800–1850Å, and 2485–2940Å are from over-exposed regions on the SWP and LWP cameras.

1976), predicted by our model fit would bring the spectroscopic mass into better agreement with the dynamical and evolutionary masses.

Our atmosphere model for α Vir predicts a hydrogen ionizing flux of $Q_0 = 7.8 \times 10^{45}$ photons s^{-1}, 1.7 times more hydrogen ionizing flux than an ATLAS9 model for the same effective temperature and gravity. Our model helium-ionizing flux is over 40 times larger than that predicted by ATLAS9. The model hydrogen-ionizing flux is closer to the ionizing flux derived from the nebular Hα emission (Reynolds 1985); nevertheless, it falls short of the measured lower limit by about a factor of two. If the effective temperature of α Vir is in the upper range established by Code et al. (1976), we find agreement between our predicted hydrogen ionizing flux and the measured lower limit. These higher effective temperatures, however, appear to the inconsistent with the observed UV flux distribution. A more detailed study of our model atmospheres of β CMa and α Vir is in preparation.

3.4. Spherical vs. Plane-Parallel Models

We find that the differences in the EUV between our models and those of Kurucz are primarily due to the differences in the temperature structures between line-blanketed spherical and line-blanketed plane-parallel models. To explore these differences, we computed a grid of models, all of which have an effective temperature of $T_{\rm eff} = 20\,990$ K, a surface gravity of $\log g = 3.2$, and turbulent velocity of $\xi = 2$ km s^{-1}. These models differ in the geometry of the calculation

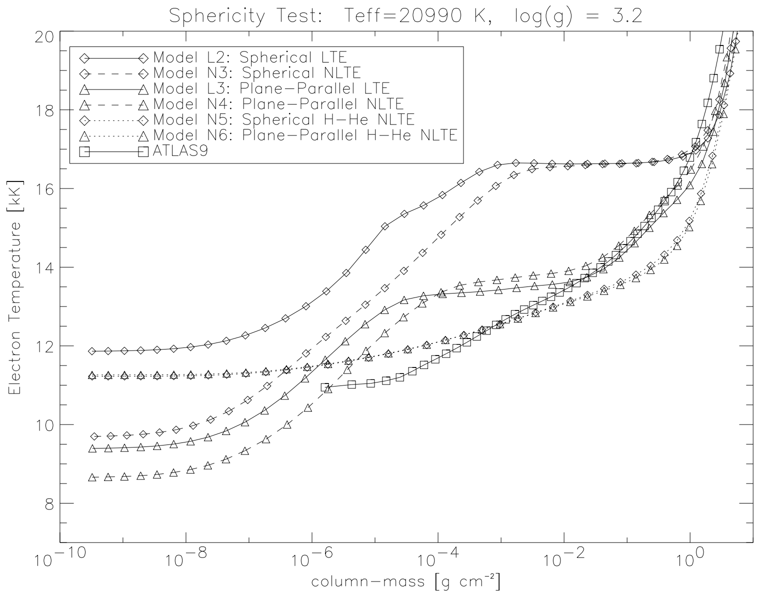

Figure 5. Temperature structures for a variety of spherical and plane-parallel models. An ATLAS9 structure is included for comparison. Spherical line-blanketed models show significantly warmer temperature structures compared with plane-parallel line-blanketed models. Non-LTE models with no metal line blanketing show identical structures for the two geometrical treatments.

(spherical or plane-parallel), the use and degree of LTE or non-LTE line blanketing, the presence or absence of LTE line scattering, the value of the outer boundary pressure, the value of the outer boundary continuum optical depth, and the resolution of the wavelength grid in the model calculation. We find that the combination of parameters in our models which has the most significant effect on the temperature structure is the inclusion of both metal line blanketing and a spherical geometry. The temperature structure, in particular the region responsible for the EUV continuum, is only slightly affected, if at all, by the outer boundary conditions, the degree of line blanketing, the presence of LTE line scattering, or the resolution of the wavelength grid.

In Fig. 5 we compare the temperature structures of six LTE and non-LTE models with and without line blanketing. The ATLAS9 temperature structure is shown for comparison. The temperature structures of the line-blanketed models fall into two groups. The spherical models show a plateau structure near 16,600 K between column masses 1 g cm^{-2} and 10^{-3} g cm^{-2}, while the plane-parallel models show a plateau structure near 13,300 K between column masses 10^{-2} g cm^{-2} and 10^{-4} g cm^{-2}. The non-LTE and LTE models have nearly the same temperature structure in these plateau regions and differ substantially only beyond the plateau at lower mass columns. The differences in the temperature structures between the two geometries have significant effects on the flux levels of the synthetic EUV continua as shown in Fig. 6.

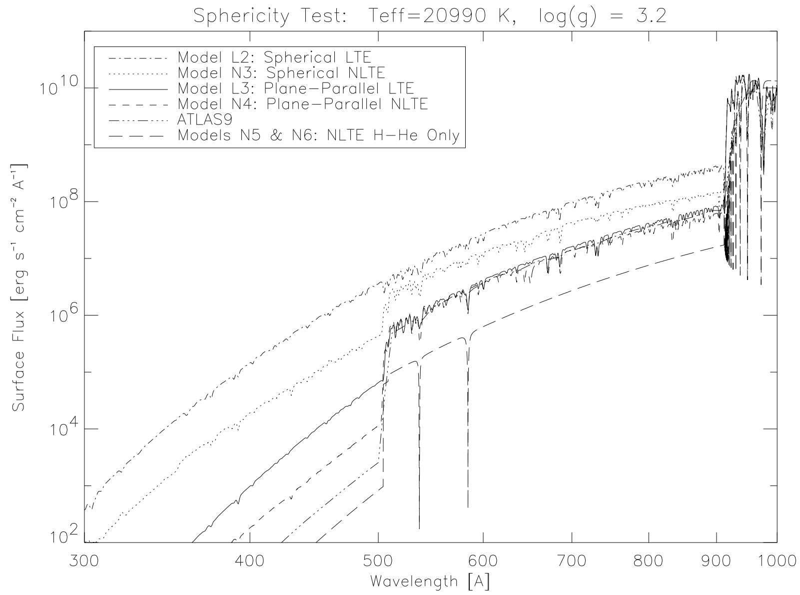

Figure 6. Synthetic spectra in the EUV for a variety of spherical and plane-parallel models. An ATLAS9 spectrum is included for comparison. Spherical line-blanketed models predict significantly larger EUV fluxes compared with plane-parallel line-blanketed models. Non-LTE line-blanketed models predict similar or lower EUV fluxes than LTE models due to the overpopulation of H I and He I ground states in the non-LTE treatment. Non-LTE models with no metal line blanketing show identical EUV spectra for the two geometrical treatments.

The Lyman continua of the non-LTE line-blanketed models form at the same column masses in the atmosphere as the LTE models, but the overpopulation of the ground states in the non-LTE models further affects the flux levels of the H I and He I Lyman continua. Our LTE, line-blanketed, plane-parallel synthetic spectrum predicts the same flux in the H I Lyman continuum as the ATLAS9 spectrum, but these models predict different flux levels for the He I continuum below 504Å. This is due to the different temperature structures predicted by these models for column masses less than 10^{-2} g cm^{-2}. We do not yet understand the reasons for the differences between the models in this region. Differences in the two codes may exist in the treatment of metal-line blanketing. In addition, important differences may exist between the two codes for the equation of state, which is computed by PHOENIX in a completely independent way from that of ATLAS9, e.g., by using different energy-level data.

The non-LTE H-He only models (N5 and N6), with no metal line blanketing, show nearly identical temperature structures and EUV spectra for both geometries. The Lyman continuum of the unblanketed pure H-He non-LTE model is more than a factor of 15 lower than that predicted by the spherical non-LTE model (N3) with metal-line blanketing. Therefore, the significant differences in the model EUV spectra for a particular treatment of the geometry are a result of the inclusion of metal-line blanketing.

Acknowledgments. The authors thank S. Shore, I. Hubeny, D. Cohen, R. Kurucz, and S. Starrfield. JPA acknowledges support from an ASU NASA Space Grant Fellowship. This work was supported in part by NASA ATP grant NAG 5-3018 and LTSA grant NAG 5-3619 to the University of Georgia, by NASA LTSA grants NAGW 4510 and NAGW 2628, NASA ATP grant NAG 5-3067 and by NSF grant AST-9417057 to Arizona State University, and by NSF grant AST-9417242, NASA grant NAG5-3505 and an IBM SUR grant to the University of Oklahoma. Some of the calculations presented in this paper were performed on the IBM SP2 of the UGA UCNS, at the San Diego Supercomputer Center and the Cornell Theory Center, with support from the National Science Foundation, and at the NERSC with support from the DoE. We thank all these institutions for a generous allocation of computer time.

References

Aufdenberg, J. P., Hauschildt, P. H., Shore, S. N., Baron, E., 1997, ApJ, submitted

Baron, E., Hauschildt, P. H., 1997, ApJ, submitted

Bohlin, R. C., Holm, A. V., 1984, IUE Newsletter, 24, 74

Cassinelli, J. P., et al., 1995, ApJ, 438, 932

Cassinelli, J. P., et al., 1996, ApJ, 460, 949

Code, A. D., Davis, J., Bless, R. C., Hanbury Brown, R., 1976, ApJ, 203, 417

Gry, C., Lemonon, L., Vidal-Madjar, A., Lemoine, M., Ferlet, R., 1995, A&A, 302, 497

Gry, C., York, D. G., Vidal-Madjar, A., 1985, ApJ, 296, 593

Hauschildt, P. H., Baron, E., Allard, F., 1997, ApJ, 483, 390

Hauschildt, P. H., Baron, E., Starrfield, S., Allard, F., 1996, ApJ, 462, 386

Hauschildt, P. H., Starrfield, S., Shore, S. N., Allard, F., Baron, E., 1995, ApJ, 447, 829

Kurucz, R. L., 1992, in The Stellar Populations of Galaxies (IAU Symp. 149), eds. R. Barbuy & A. Renzini (Kluwer, Dordrecht), p. 225

Kurucz, R. L., 1994, Atomic Data for Opacity Calculations, CD-ROM No. 1

Najarro, F., Kudritzki, R. P., Cassinelli, J. P., Stahl, O., Hillier, D. J., 1996, A&A, 306, 892

Popper, D. M., 1980, ARA&A, 18, 115

Reynolds, R. J., 1985, AJ, 90, 92

Schaerer, D., de Koter, A., 1997, A&A, 322, 598

Schaller, G., Schaerer, D., Meynet, G., Maeder, A., 1992, A&AS, 96, 269

Smalley, B., Dworetsky, M. M., 1995, A&A, 293, 446

Watson, R. D., 1972, ApJS, 24, 167

Welsh, B. Y., 1991, ApJ, 373, 556